

# Subsecond Model Updating for High-Rate Structural Health Monitoring

Michael Carroll<sup>1</sup>, Austin Downey<sup>1,2</sup>, Jacob Dodson<sup>3</sup>, Jonathan Hong<sup>4</sup> and James Scheppegrell<sup>4</sup>

<sup>1</sup>Department of Mechanical Engineering  
University of South Carolina

<sup>2</sup>Department of Civil and Environmental Engineering  
University of South Carolina

<sup>3</sup> Air Force Research Laboratory

<sup>4</sup> Applied Research Associates

## ABSTRACT

High-rate monitoring, condition assessment, and control of structural systems experiencing high-rate dynamics is challenging due to these structures experiencing events of timescales below 10ms. Examples of structures that require high-rate structural health monitoring include spacecraft, hypersonic vehicles, ballistic packages, and active barriers for blast mitigation. Subsecond model updating techniques for this unique class of structures must be capable of tracking the system through rapidly changing input forces and time-varying structural parameters. Moreover, any methodology designed for high-rate structural health monitoring must account for the challenges associated with high-speed data measurement and model updating in its formulation. This work presents and experimentally validates a subsecond model updating methodology for enabling high-rate structural health monitoring of a structure that undergoes system-level changes (i.e., damage) while accounting for uncertainties in the measurements, model, and system. To achieve this, a parallelized residual minimization model updating technique is implemented on an FPGA where model parameters are drawn from a continuously updated parameter pool. The parameter pool is updated based on previous system states and known upcoming events (e.g., impacts). In this work, the DROPBEAR experimental test bed at the Air Force Research Laboratory is used to validate the proposed methodology for a one-degree-of-freedom system with a continuously changing boundary condition. Results demonstrate that a continuously changing boundary condition can be successfully tracked at time intervals of 10 ms or less. Computational speed, prediction accuracy as a function of model size, and the role of measurement noise are examined in this work.

**Keywords:** real-time model updating, finite elements analysis, structural health monitoring, high-rate dynamics

## INTRODUCTION

The development of real-time modeling methods for structures undergoing high-rate dynamics is driven by the demand to develop active structures. Examples of active structures that experience high-rate dynamics include active blast mitigation barriers, ballistics packages, and hypersonic vehicles [1, 2, 3, 4]. The end goal of such development is the monitoring and mitigation of high-speed impacts and shock events on structures in real-time. For example, a 1 ms delay in a decision made for a ballistic package traveling at Mach 5 would result in the package being 1.7 meters down range. Due to the timescales considered, the monitoring and condition assessment of structures must occur at the single-digit millisecond timescale.

Due to the unmodeled nature of the structures operating in these harsh environments that are currently unprecedented, a model updating technique cannot rely on pre-calculated data sets. This paper presents an algorithm capable of real-time model updating and experimentally validates the algorithm using a test structure. The algorithm leverages an error minimization technique in the frequency domain to develop a methodology that can operate with the desired single-digit millisecond timescales while producing accurate estimation of parameter changes in the test structure.

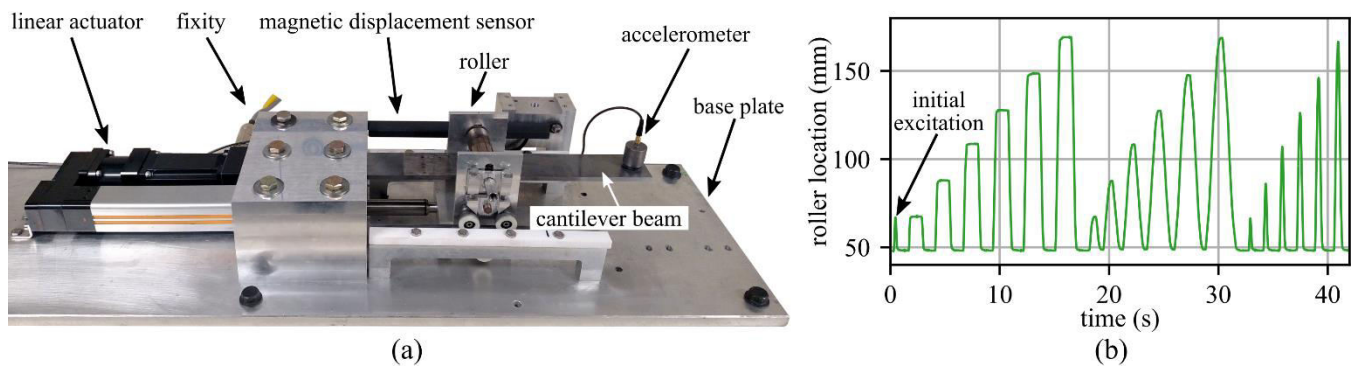


Figure 1: The Dynamic Reproduction of Projectiles in Ballistic Environments for Advanced Research (DROPBEAR) experimental test bed showing: (a) key components; and (b) the test profile of the roller movement used in this work.

## BACKGROUND

The DROPBEAR (Dynamic Reproduction Of Projectiles in Ballistic Environments for Advanced Research) experimental setup was first introduced by Joyce et al. [5] and is presented in Figure 1(a). It was designed with two user-controlled parameters: a detachable mass and a continuously variable roller cart, where the detachable mass represents a discrete system change (i.e. damage) and the movable roller a system change. For the experiments conducted in this work, the roller cart was used to simulate a progressive change in the structure and the mass drop was not utilized.

The experimental test bed features a large, rectangular aluminum base securely affixed to a base plate. This plate serves as the mounting base for the clamp housing in which the cantilever beam is secured. The beam is made from steel and dimensioned with a width of 51 mm (2 in), a free length of 350 mm (13.81 in), and a thickness of 6.3 mm (0.25 in). One single-axis PCB Piezotronics 393B04 accelerometer was attached to the beam at 337 mm (13.27 in) from the primary clamp (Figure 1(a)). The accelerometer was connected to a 24-bit IEPE ADC NI-9234 housed in a National Instruments (NI) cDAQ-9172 eight-slot chassis. A NI PXIe-8880 controller placed in the chassis was used for real-time data acquisition and processing using custom LabVIEW codes.

A Parker Drive linear actuator is used to control the location of the cart, and can be programmed with predetermined courses of motion [6]. Once programmed, the actuation of the cart was triggered using NI-LabVIEW through a digital output signal from a NI PXI-6133. The excitation of the beam was generated by the cart motion along the beam length as the sole input force into the system (Figure 1). A LabVIEW program acquired and saved response data from an accelerometer. The estimated cart position was verified through a Honeywell Sensing and Productivity Solutions magneto-resistive linear transducer, model number SPS-L225-HALS. The analog voltage input from the linear transducer was acquired through LabVIEW via a 14-bit ADC NI PXI-6133 coupled with an NI TB-2709. MATLAB and Python were employed for post-processing of data to perform modal analysis.

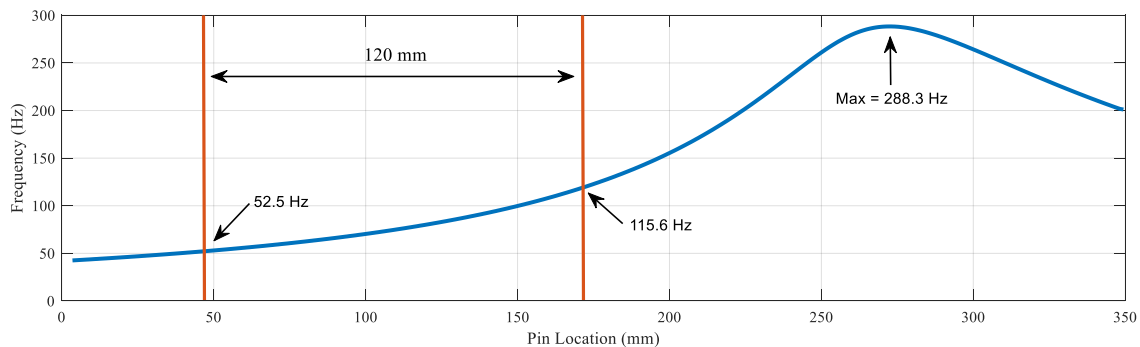
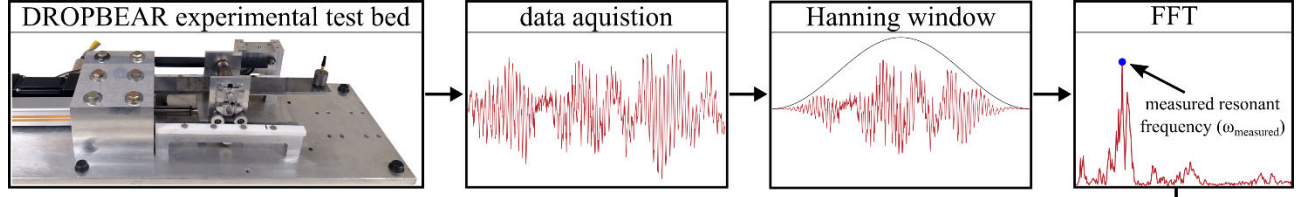


Figure 2: Comparison of first frequency mode with changing pin location. The mode is from the finite element model using Python. For the experimental data, initial and final frequencies for the pin location are shown.

## Experimental



## Analytical

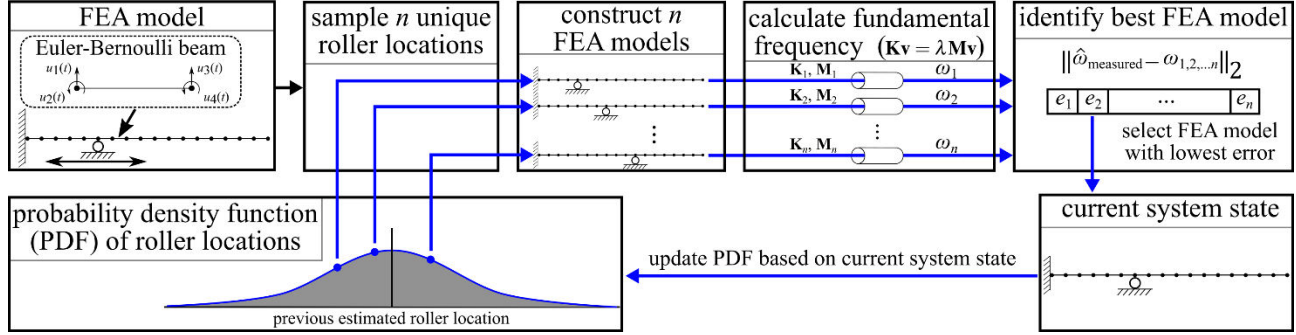


Figure 3: Diagram showing the flow of the millisecond model updating method.

The development of a numerical study for the changing parameters based on a finite element analysis (FEA) code revealed how the natural frequencies and mode shapes change linearly with changes in the cart position, as presented in Figure 2 and discussed in detail in [7]. Due to the redundancy in the natural frequency of the beam during the cart's full travel along the beam, the roller movement was limited to the range of 48 mm to 168 mm from the fixed end.

The proposed algorithm is presented in Figure 3. The algorithm functions by acquiring data from the accelerometer, performing a fast Fourier transform (FFT), and generating a value for the first frequency. Additionally, an Euler-Bernoulli FEA (Finite Element Analysis) model, implemented in LabVIEW, is used as the model to be updated in real-time. The FEA model has a specified number of unique cart locations at which the natural frequency can be calculated. To enable real-time model-updating without pre-calculated data sets, these FEA models are solved in real-time. Modal analysis is used to calculate the structure's natural frequency, where the damping term ( $C$ ) can be disregarded due to an insignificant contribution of damping within the system. Therefore, we employ the following free vibration equation of motion:

$$\ddot{M}\ddot{x} + Kx = 0 \quad (1)$$

This solution can be further simplified by making the assumption that for the harmonic solution  $x_n = \Phi_n \sin(\omega_n t)$  where  $\Phi$  represents the mode shapes of the solution and  $\omega_n$  is the undamped natural frequency. Upon substitution, where  $\Phi = 0$  is a trivial solution, the equation becomes:

$$(-\omega^2 M + K)\Phi = 0 \quad (2)$$

The solution of interest is where the natural frequencies  $\omega$  and modes  $\Phi$  that satisfy the generalized eigenvalue problem, where  $\lambda_n = \omega_n^2$ , results in the equation:

$$K\Phi = \lambda M\Phi \quad (3)$$

Within this equation,  $\lambda$  is the diagonal matrix of eigenvalues and  $\Phi$  are the associated eigenvectors where  $\omega_n = \sqrt{\lambda_n}$ . Therefore, the undamped natural frequency can be solved for using the generalized eigenvalue problem and selecting the lowest valued eigenvalue.

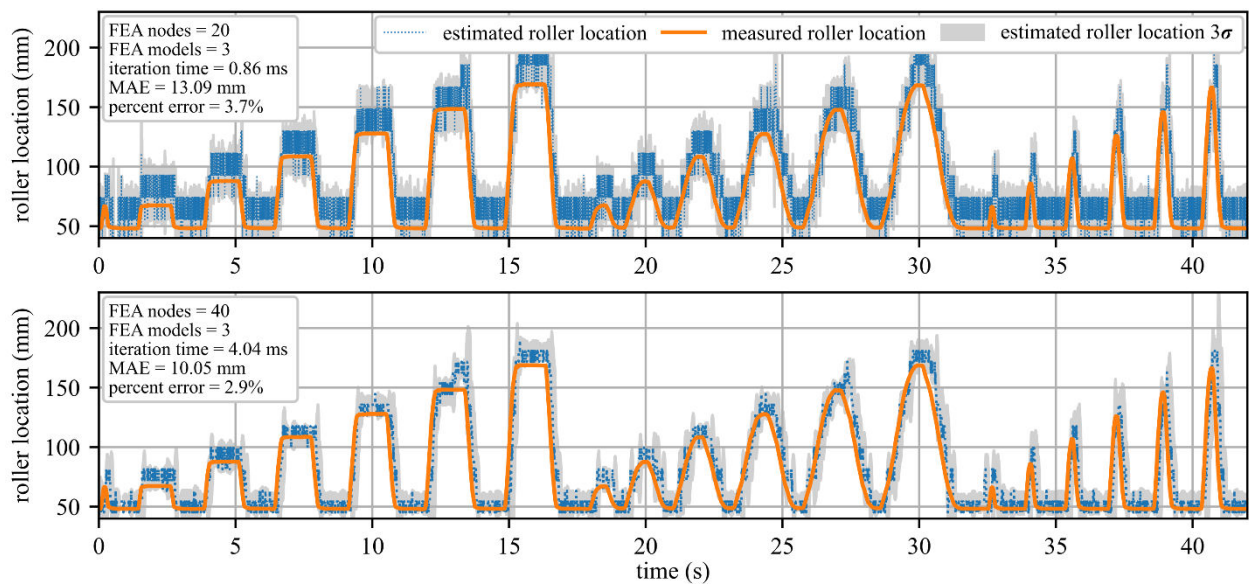


Figure 4: 20 and 40 node FEA models, each with three parallel instances of FEA models being solved, are shown with temporal data responses.

For each sampled pin location, a unique  $\mathbf{M}$  and  $\mathbf{K}$  matrix was generated. In order to calculate each pin location's unique first natural frequency, LabVIEW's Cholesky factorization and Jacobi Method of decomposition were employed to calculate the appropriate eigenvalues associated with the FEA model. Each FEA model's unique first frequency was compared against the FFT's first frequency acquired by the accelerometer data. The pin location associated with the FEA model frequency of least error would become the mean around which the next number of unique pin locations are centered using a Gaussian probability density function (PDF) as presented in Figure 3.

### ANALYSIS

The results for the experimental test when implementing the DROPBEAR test bed will be discussed with consideration to real-time model updating techniques described in the preceding background section of this paper.

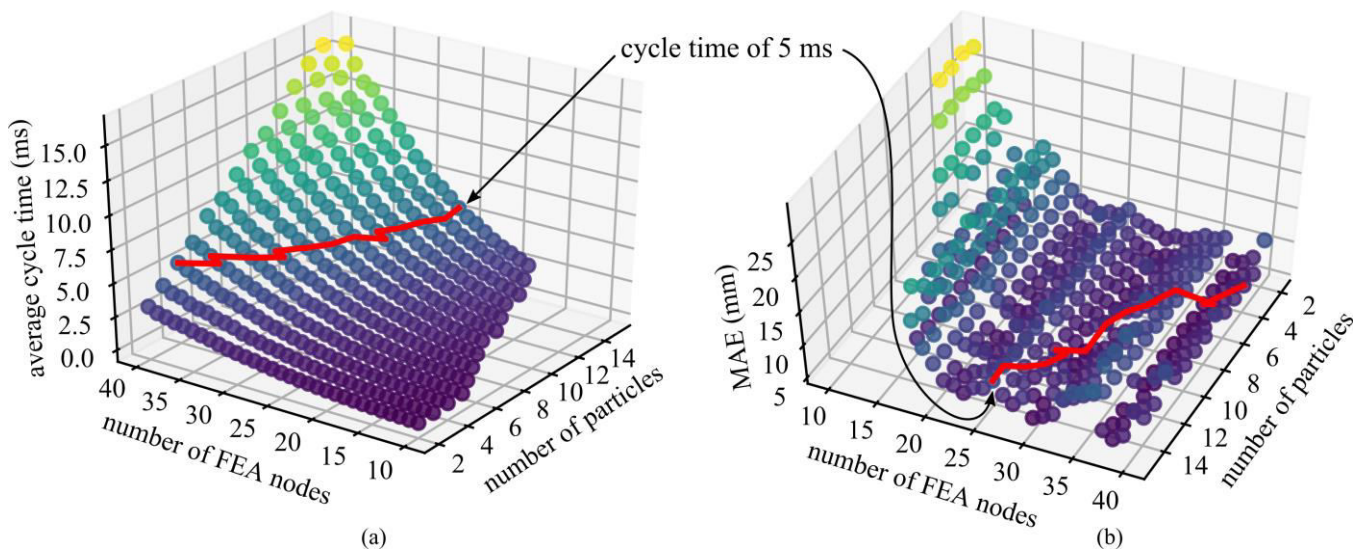


Figure 5: 233 Results of automated tests displaying the: (a) average iteration time for each possible combination, (b) mean absolute error for each combination. Note: There is a reversal of the axes numbering to aid plotting.

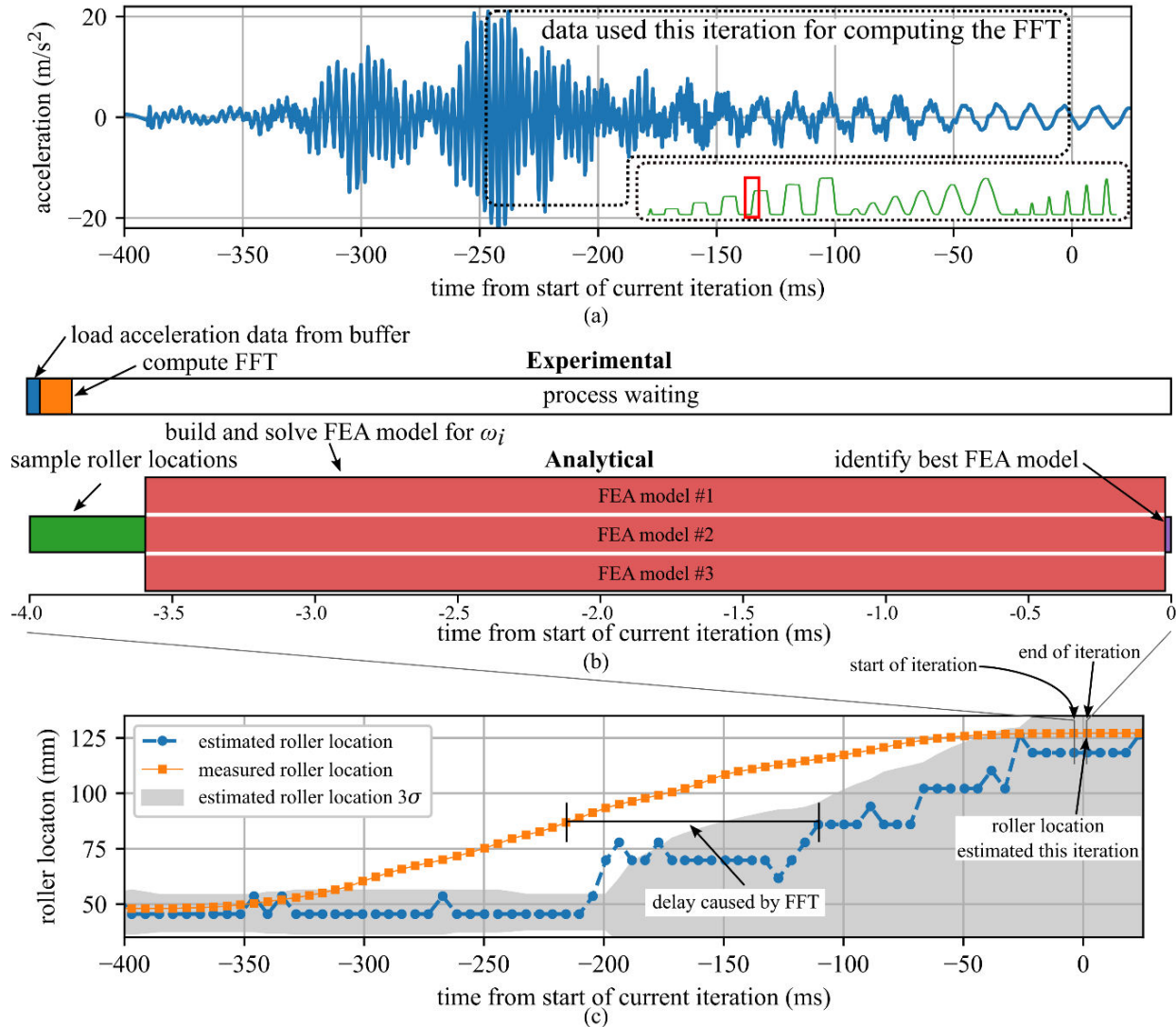


Figure 6: Timing of the experimental setup for one instance of the flowchart in Figure 3 showing the: (a) raw acceleration data from the leading step roller movement, (b) experimental and analytical algorithm calculations, (c) comparison of roller location.

When increasing the number of nodes in the FEA model, there is an increase in the accuracy of the position estimation. However, this increase in accuracy results in an increase in computation time as well. For example, when using an FEA model of 20 nodes and 40 nodes, there was an accuracy of 3.9% and 2.9% with a computational speed of 0.86 ms and 4.04 ms, respectively (Figure 4). To further represent this contrast of speed with varying FEA node size and simultaneous instances within the algorithm, every combination of FEA nodes ranging from 10 to 40 and the number of FEA models from 3 to 15 were experimentally tested as represented in Figure 5(a). As previously stated, the increase in the number of FEA nodes results in an increase in error reduction demonstrated as MAE (Mean Absolute Error) and represented in Figure 5(b). However, there is no reduction in the error when increasing the number of simultaneous FEA models (number of particles) as the roller position speed was limited by the linear actuator speed of 250 mm/s. The red lines in Figure 5 indicate the 5 ms line which represents the results showing a comparison to the proposed computation speed of <10 ms.

The next issue to be addressed to understand the results is the lag associated with when the measurement is taken from the accelerometer, the FFT is computed. The data being windowed results in a final roller location estimation that is designated as the 0 ms position (Figure 6(a)). The analytical portion of the algorithm selected resulted from using three parallel 40 node FEA models constructed from three continuously selected roller positions for each iteration of the model updating described in the aforementioned flowchart in Figure 3. During the analytical portion of this computation, the majority of the

computation time expended is derived from FEA models solving for the generalized eigenvalue problem of the modal analysis. However, the time taken to load the data from the buffer and perform the FFT during the experimental portion is relatively short by comparison (Figure 6(b)). This overall computation cost is further displayed in Figure 6(c), where the total sliding window for data acquisition and processing consumes roughly 198 ms.

## CONCLUSION

Challenges are associated with high-rate monitoring, condition assessment, and control of structural systems experiencing high-rate dynamics events below 10 ms timescales. The DROPBEAR test bed at the Air Force Research Laboratory has proven valid in serving as an experimental test bed for validating algorithms capable of real-time modeling of a continuously variable parameter in the form of changing roller cart movement. The algorithms discussed in this paper used real-time computation without the use of pre-calculated datasets and performed a frequency-based error minimization technique, which compared an experimentally derived resonant frequency to parallel instances of a FEA model with varying parameters. Furthermore, this comparison between experimental and analytical values resulted in the value with the highest agreement selected as the system's current state and offered as the next value in a pool that is sampled without replacement for further iterations of the algorithm.

Numerical verification proved that an increase in the FEA model's fidelity and simultaneous instances resulted in decreased error in the cart location estimation. However, as average cycle times for each iteration increases, error reduction decreases. Proving the capability of the selected algorithm to operate at the proposed <10 ms timescale, results demonstrated that a 40-node FEA model ran in three separate parallel instances was capable of updating every 4.04 ms with an accuracy of 2.9%.

## ACKNOWLEDGEMENTS

This material is based upon work supported by the United States Air Force through the Air Force Research Laboratory Summer Internship Program and AFRL/RWK contract number FA8651-17-D-0002 and partly by the National Science Foundation Grant No. 1850012 and 1937535. The support from these agencies is gratefully acknowledged. Any opinions, findings, and conclusions or recommendations expressed in this material are those of the authors and do not necessarily reflect the views of the United States Air Force or the National Science Foundation.

## REFERENCES

- [1] H. Wadley, K. Dharmasena, M. He, R. McMeeking, A. Evans, T. Bui-Thanh, R. Radovitzky, An active concept for limiting injuries caused by air blasts, *International Journal of Impact Engineering* 37 (3) (2010) 317–323. doi:10.1016/j.ijimpeng.2009.06.006. URL <https://doi.org/10.1016/j.ijimpeng.2009.06.006>
- [2] J. C. Dodson, R. D. Lowe, J. R. Foley, C. Mougeotte, D. Geissler, J. Cordes, Dynamics of interfaces with static initial loading, in: *Dynamic Behavior of Materials, Volume 1*, Springer International Publishing, 2013, pp. 37–50. doi:10.1007/978-3-319-00771-7\_5. URL [https://doi.org/10.1007/978-3-319-00771-7\\_5](https://doi.org/10.1007/978-3-319-00771-7_5)
- [3] C. Stein, R. Roybal, P. Tlomak, W. Wilson, A review of hypervelocity debris testing at the air force research laboratory, *Space Debris* 2 (4) (2000) 331–356. doi:10.1023/b:sdeb.0000030024.23336.f5. URL <https://doi.org/10.1023/b:sdeb.0000030024.23336.f5>
- [4] W. Chen, H. Hao, Numerical study of blast-resistant sandwich panels with rotational friction dampers, *International Journal of Structural Stability and Dynamics* 13 (06) (2013) 1350014. doi:10.1142/s0219455413500144.
- [5] B. Joyce, J. Dodson, S. Laflamme, J. Hong, An experimental test bed for developing high-rate structural health monitoring methods, *Shock and Vibration* 2018 (2018) 1–10. doi:10.1155/2018/3827463. URL <https://doi.org/10.1155/2018/3827463>
- [6] Parker Servo Systems. 2016, onexia.com/parker/pdf/ONExia-Parker-P-Series-Catalog.pdf.
- [7] J. Hong, J. Dodson, S. Laflamme, A. Downey, Transverse Vibration of Clamped-Pinned-Free Beam with Mass at Free End, *Applied Sciences* 2019, 9(15):2996. doi:10.3390/app9152996. URL <https://doi.org/10.3390/app9152996>